Soft X-Ray Spectra of High Temperature Argon Plasma for Potential Cell Treatment
(Spektrum X-Ray Lembut Plasma Argon Suhu Tinggi untuk Rawatan Sel Berpotensi)

Poh Hun Seng[1], Yap Seong Ling[1,*], Teow Sin Yeang[2,3], Tan Han Yi[1] & Yap Seong Shan[4]

[1]Plasma Technology Research Centre, Department of Physics, Faculty of Science, Universiti Malaya, 50603 Kuala Lumpur, Malaysia

[2]Department of Biology, College of Science, Mathematics, and Technology, Wenzhou-Kean University, Ouhai, Wenzhou, China 325060

[3]Department of Biological Sciences, College of Science, Mathematics, and Technology, Kean University, Union, New Jersey 07083

[4]Department of Physics, Xiamen University Malaysia, 43900 Sepang, Selangor, Malaysia

ABSTRACT

A plasma pinch is created when the current sheath collapses onto the axis in a plasma focus discharge. The plasma focus produces a high temperature and high density plasma, emitting soft x-ray with energy in the range of kiloelectronvolt. The soft x-ray is suitable for the radiography of biological samples, or as the source for microscopy or absorption spectroscopy of tissues which are not visible to conventional x-ray. Similar sources are available only from synchrotron radiation facilities with fairly low brightness. The argon plasma pinch produced by a plasma focus was investigated. The x-ray spectra was resolved with a set of filtered detector for the range of 1 to 20 Å. The plasma electron temperature measured was within 3 keV to 10 keV, with typical plasma density of 10^{19}/cm^3. The discharge energy of 1.5 to 2.5 kJ at 1 mbar argon measured a peak current of 95 kA to 122 kA, and total soft x-ray energies of 22 to 52 J.

Keywords: Argon plasma; plasma focus; plasma pinch; soft x-ray; x-ray spectra

ABSTRAK

Jepitan plasma dihasilkan apabila sarung semasa runtuh ke paksi dalam nyahcas fokus plasma. Fokus plasma menghasilkan suhu tinggi dan plasma ketumpatan tinggi, memancarkan sinar-x lembut dengan tenaga dalam julat kiloelektronvolt. Sinar-x lembut sesuai untuk sampel biologi radiografi atau sebagai sumber untuk mikroskopi atau spektroskopi penyerapan tisu yang tidak boleh dilihat oleh sinar-x konvensional. Sumber yang sama hanya tersedia daripada kemudahan sinaran sinkrotron dengan kecerahan yang agak rendah. Jepitan plasma argon yang dihasilkan oleh fokus plasma telah dikaji. Spektrum sinar-x telah diselesaikan dengan satu set pengesan yang ditapis untuk julat 1 hingga 20 Å. Suhu elektron plasma yang diukur adalah dalam lingkungan 3 keV sehingga 10 keV dengan ketumpatan plasma biasa 10^{19}/cm^3. Tenaga nyahcas 1.5 hingga 2.5 kJ pada 1 mbar argon mengukur arus puncak 95 kA hingga 122 kA dan jumlah tenaga sinar-x lembut 22 hingga 52 J.

Kata kunci: Argon plasma; fokus plasma; jepitan plasma; spektrum sinar-x; sinar-x lembut

INTRODUCTION

The argon plasma is produced by a plasma focus (PF) discharge with a high current driven to form a pinch through the coaxial electrode geometry. The PF devices were invented in 1960 for fusion research in two configurations independently by Mather (1965) and Filippov, Filippova and Vinogradov (1962) with unique difference in their electrode length to anode diameter ratio. Mather type of PF has a longer electrode allowing an axial acceleration phase to take place while shock

heating the gas to high temperature. The Mather type PF incorporating a hollow anode produced intense x-ray from the gas forming plasma (Poh et al. 2020). Filippov PF has a longer radial phase produced plasma pinch often containing anode material (Filippov et al. 1996). The Mather type PF used here works on a fast-discharging energy storage capacitor bank connected to its electrode system through a spark-gap switch. A current sheath was formed at the base of the cathode upon discharge and driven by the Lorentz force to the anode tip, and subsequently compressed into a cylindrical plasma pinch. During the pinch phase, several kinds of radiation are produced and they were accounted by the complex dynamics in the pinch (Kubes et al. 2023). The high energy density pinch plasma emitting multiple radiations, including pulsed ion beams (Akel et al. 2022; Bhuyan et al. 2005; Lim et al. 2021), electron beams in the reverse direction (Patran et al. 2005; Zhang et al. 2007), soft and hard x-rays (Ay 2021; Castillo-Mejía et al. 2001; Housley et al. 2021; Kalaiselvi 2016; Mohammadi et al. 2017), and neutrons from thermonuclear and non-thermonuclear reactions (Yap et al. 2005).

The early research of PF focused on the nature of the device and its capability in producing neutrons (Bernard et al. 1977) that has made PF an unique device as a neutron source for various neutron irradiation application (Benzi et al. 2004; Bernard et al. 1977; Verma et al. 2008). The PF pinched plasma is also an intense source of energetic particles and x-ray. Reports shown that a soft x-ray yield could be in the range of 6 J/shot (Mohammadi et al. 2017) or 35.9 J/shot (Patran et al. 2005) from different devices. The high intensity of the x-ray emission was used to demonstrate a fine resolution radiograph (Castillo-Mejía et al. 2001). The x-ray source has good potential for medical applications, with a high dose rate greater than 10^8 Gy/s and could be operated repetitively, demonstrated for interstitial radiosurgery (Tartari et al. 2004), and medical imaging (Miremad & Bidabadi, 2018). PF produced hard x-ray of an average dose of (1.5 ± 0.1) mGy/sr per shot within an angular positions $\pm 70°$, was used for industrial radiography (Knoblauch et al. 2018). The irradiation effects on surface tumours by plasma focus x-ray was experimentally verified on nude mice (Isolan et al. 2019). A high dose of 1 Gy transferred from fast pulsed x-ray was found suitable for radiotherapy (Sumini et al. 2019), and the potential application of the plasma soft x-ray on cancer treatment was discussed by several authors (Jain et al. 2021; Poh et al. 2020).

EXPERIMENTAL SETUP AND DIAGNOSTIC TECHNIQUES

In this study, a Mather type PF powered by a single capacitor was employed. The capacitor bank was charged at 10 kV to 13 kV, giving the discharge energies range from 1.5 kJ to 2.5 kJ. Argon was filled to the PF as the single working gas. The pressure in the discharge chamber was maintained at 1 mbar. The plasma focus chamber enclosed the coaxial electrode; being a set of six coaxial outer electrodes (cathode) arranged concentrically around an inner electrode (anode) which are electrically separated at the back wall by an insulating sleeve. A schematic showing the PF setup and the electrical diagram is presented in Figure 1.

A Rogowski coil was placed around the anode to measure the discharge current and a high voltage probe measured the discharge voltage of the PF tube acrossed the anode and cathodes. The Rogowski coil and high voltage probe used here were similar to that reported previously (Lim et al. 2016). The current and voltage signals registered provided information of the plasma dynamics and the characteristic of the plasma pinch. In addition to the measurement of discharge voltage and current, two diagnostic ports were employed, one at the side-on direction and another one at the end-on direction both facing the plasma pinch generated above the anode. At the side-on direction, the time-resolved x-ray spectra was measured by the PIN5 detector. The PIN5 detector was essentially an array of five filtered PIN detectors. Each detector was made by a BPX-65 PIN diode with a fast response and high sensitivity silicon layer. It has a 1.00 mm^2 radiant sensitive area giving an almost flat response between 1 and 20 Å, enabling the measurement of soft x-ray of below 10 keV. This was made possible by removing the PIN diode's original glass windows. The schematic layout of the five identical PIN diodes is shown in Figure 2. A set of Ross filters were used to provide selectivity of the transmitted x-ray specta. The measured data gave the time resolved x-ray signals and the plasma temperature, estimated from the ratio of transmitted spectra (van Paassen 1971). Table 1 show the filters used in PIN5 detector consisting the five channels, labelled as X1 to X5.

SPECTRA ANALYSIS OF X-RAY

The spectra obtained from the pinched plasma consisted of the continuum emission and line emission produced by the argon plasma, depending on the density and the temperature of the plasma. The electron temperature
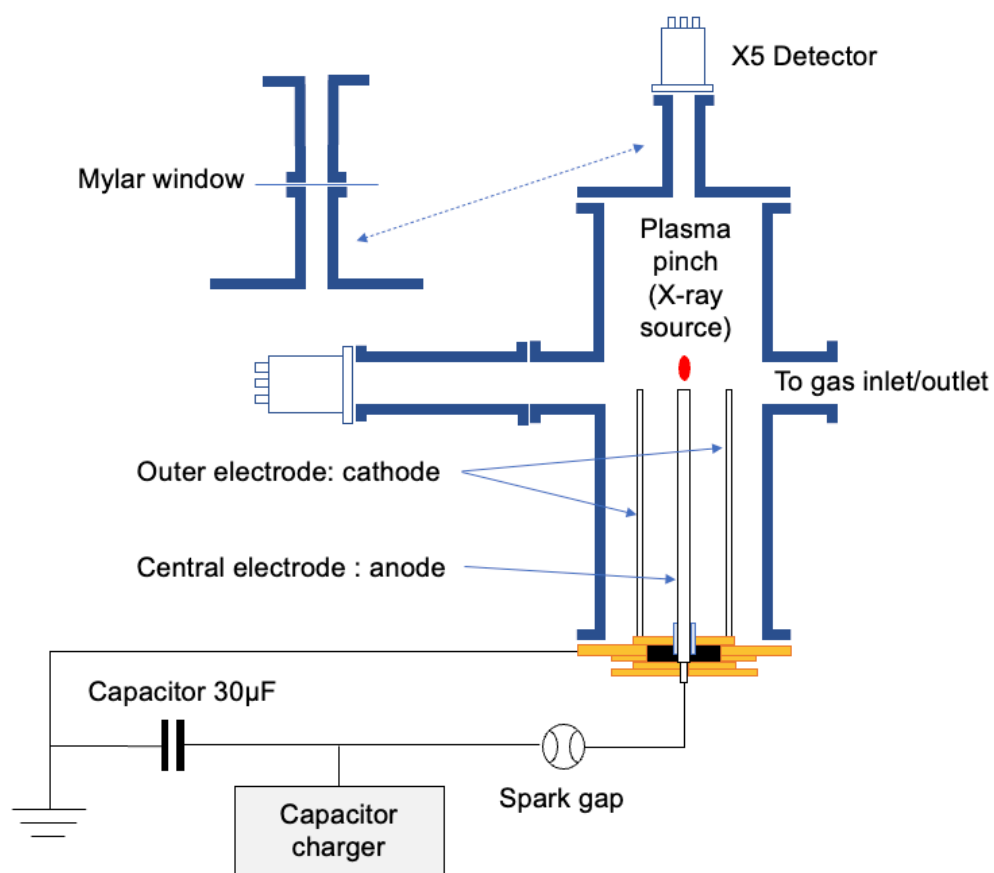
FIGURE 1. The electrical diagram and schematics of plasma focus setup
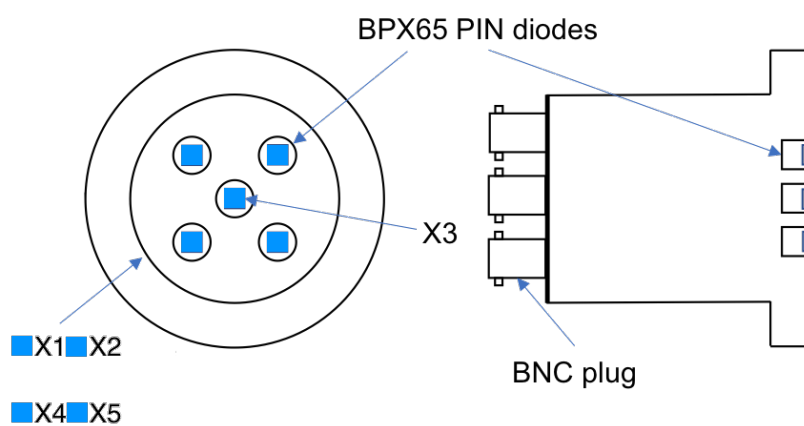

FIGURE 2. The PIN5 detector with five channels of filtered PIN diodes

of the continuum emission (Bremsstrahlung and recombination) could be calculated from the ratio of the transmitted spectra by a pair of Ross filters (Jahoda et al. 1960). The sensitivity of the PIN diodes was cross-calibrated *in-situ* with only a single layer of aluminized Mylar to cut off the visible wavelengths.

Subsequently, the PIN diode detector was prepared with the combination of the Ross filters with specific thicknesses for the five channels, labelled as X1 to X5, as listed in Table 1. The set of filters were designed to allow resolution of the plasma electron temperature of below 10 keV. The sensitivity of the channels with the filters folded in is shown in Figure 3.

TABLE 1. PIN5 detector with five channels of PIN diodes each with a combination of filters

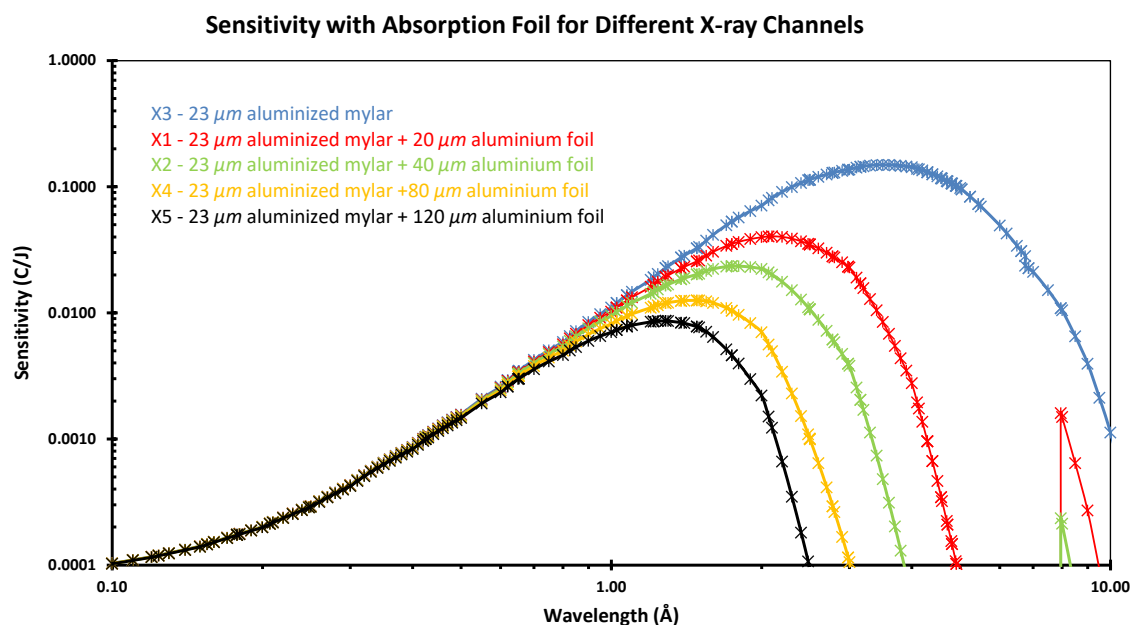| PIN diode	Filter	Thickness (μm)
X3	Aluminized Mylar	23
X1	Aluminized Mylar + aluminium foil	23+20
X2	Aluminized Mylar + aluminium foil	23+40
X4	Aluminized Mylar + aluminium foil	23+80
X5	Aluminized Mylar + aluminium foil	23+120

FIGURE 3. Sensitivity of PIN5 detector with respective filters

The spectra of argon plasma was measured by the PIN5 detector, and the ratio of x-ray was calculated by taking X1, X2, X4, X5 over the reference channel, X3. Calculated transmission of Breamstrallung spectra of argon plasma at different temperatures were obtained, similar method as that used for theta pinch plasma.

PLASMA FOCUS DISCHARGE CHARACTERISTICS

The Lee code (Lee 2014) was employed to estimate the PF discharge efficiency. The code (version RADPFV5.15de) calculated the x-ray emitted considering the energy loses through Bremsstrahlung and line radiation, included the effect of plasma self-absorption. The experimental measured data for argon plasma focus discharge from 0.8 mbar to 2 mbar were fitted with the Lee code, and obtained the four discharge parameters being the mass swept-up factor (massf for axial phase and massfr for radial phase), and current flow factor (currf and currfr). The fitted current waveform is shown in Figure 4, superimpose on a set of the measured current and voltage signals.

The computed parameters corresponding to the performance of the discharge at different pressures are listed in Table 2. The four parameters obtained were the same at different filling pressure indicated the PF discharge consistently carried a mass swept of 2% and current swept of 55% in the axial phase. The corresponding emission from the discharge were obtained from the numerical experiment using the Lee code, and to be compared with the measured data.
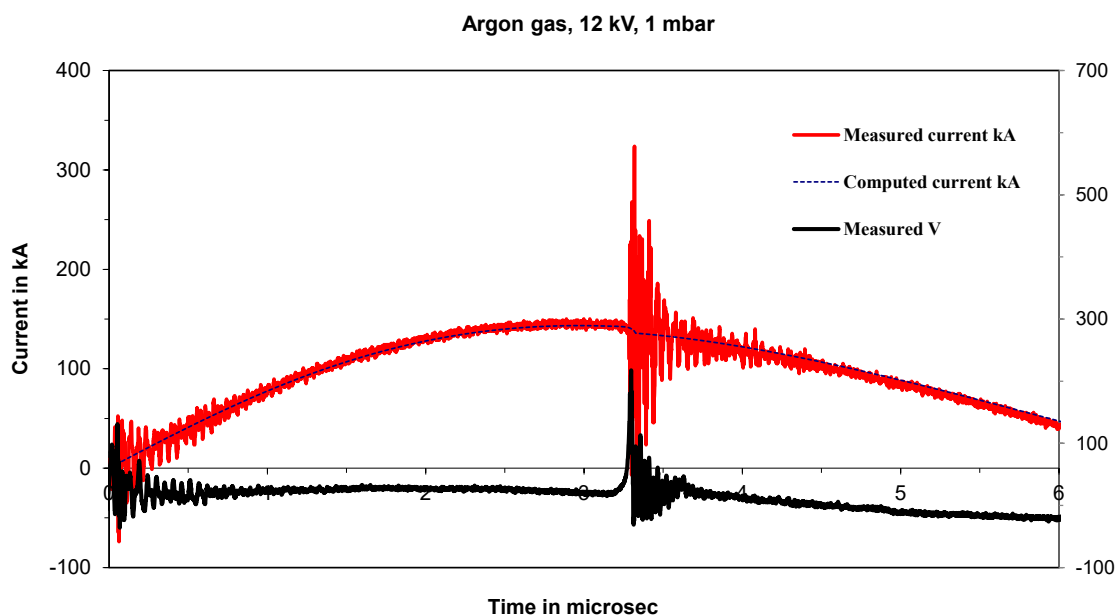

FIGURE 4. Computed current waveform fitted to the measured signals

TABLE 2. Computed parameters for argon at pressure 0.8 mbar to 2 mbar

Pressure / mbar	massf	currf	massfr	currfr
0.8	0.02	0.55	0.4	0.58
1	0.02	0.55	0.4	0.58
1.5	0.02	0.55	0.4	0.58
2	0.02	0.55	0.4	0.58

CELL SELECTION AND CYTOTOXICITY ASSAY

The impact of the argon emission on skin cells was studied. The radiation effects on cell lines was accessing on both a normal cell line and a cancer cell line; the Normal Human Dermal Fibroblasts (NHDF) cell and Skin melanoma cell (B16-F10). Cytotoxicity assays method used to measure the ability of cytotoxic compounds to cause cell damage or cell death was employed. The CellTiter 96® AQueous One Solution Cell Proliferation Assay were used to check the cell viability/proliferation (MTS assay) according to the manufacturer's instruction. Firstly, 5000 cells lines per well (100 µL/well) were seeded onto a 96-well plate and incubated overnight at 37 °C in a 5% CO_2 incubator. The next day, the cell lines were irradiated by the PF plasma produced x-rays. Culture media were drained and the culture plate containing cells was directed towards the X-ray source for plasma treatment. After the plasma irradiation, fresh culture media were added to each well and the plate was incubated for 72 h at 37 °C in the 5% CO_2 incubator. Then, 20 µL MTS reagent per well was added into the plate and incubated for additional 3 h at 37 °C in the 5% CO_2 incubator. The optical density (OD) was then measured at 490 nm using a multimode microplate reader (Tecan, Switzerland). The dose response graph was plotted by calculating the percent cell viability using the formula herewith:

$$\% \ Cell \ viability = \frac{OD \, of \ sample \ well \ (mean)}{OD \, of \ control \ well \ (mean)} \times 100$$

Statistical analysis was performed, the data was expressed in mean + standard deviations, One-way ANOVA with Dunnett's test was performed to determine the significance level using IBM Statistical tool (Version 28). P value of less than 0.05 was considered significant.

RESULTS AND DISCUSSIONS

X-RAY SPECTRA OF ARGON PLASMA

The time-resolved x-ray spectra was obtained by the PIN5 detector. A typical set of data shown in Figure 5, with X3 having hardest signal. The other channels were filtered by aluminium of different thicknesses, reduced the measured signal correspondingly. The reduction
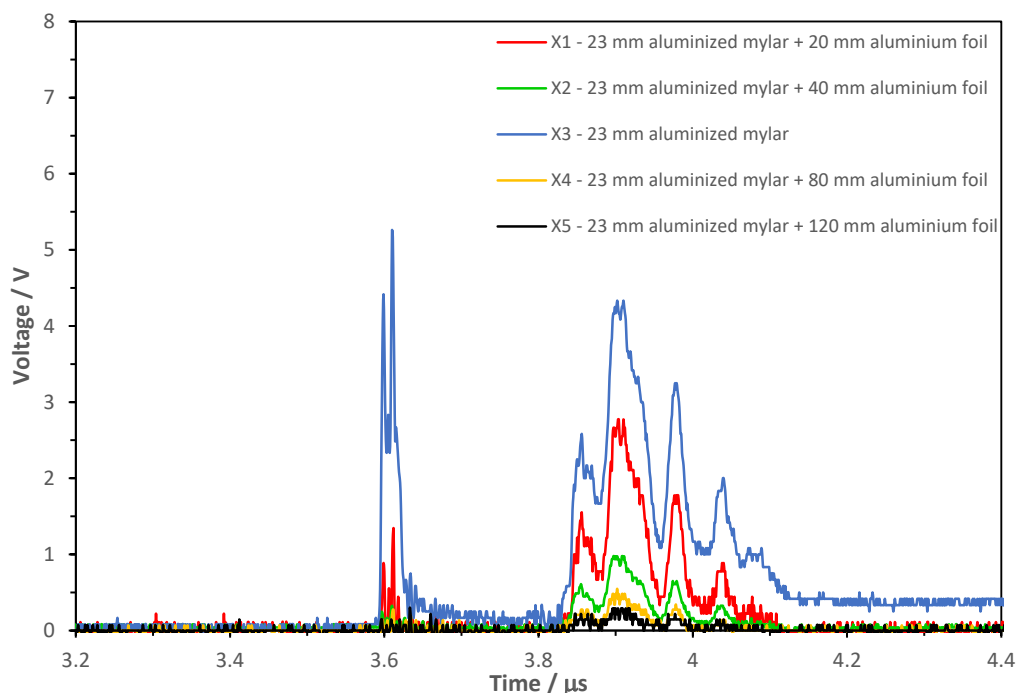

FIGURE 5. Time resolved signals of the PIN5 detector

of x-ray signals progressively with the thickness of the aluminium filters indicated a broad spectra of the x-ray emission. Major reduction by the 40 μm of aluminium filter, correspond to energy of below 5 keV. The multipeaks were correlated to the dynamics of the pinch, corresponded to the multiple dips in current signals. The spread of the multiple peaks was about 300 ns. The peaks were the transmitted intensities, that would be used to calculate the corresponding electron temperatures.

The time resolved x-ray signals obtained at the 10 kV to 13 kV charging voltage were integrated to give the total x-ray photon energies. The total average x-ray photon energy increased linearly with the charging voltage, that the highest x-ray photon energy of 52 J measured at 13 kV. Similar conditions were used in the numerical experiment using the Lee code to give the total energy released correspond to the x-ray emission. The comparision between measured results and that from

the numerical experiments is shown in Figure 6. The calculated yield shown a same trend with experiments; higher x-ray yield with higher applied voltage, but overall with slightly lower value. At discharge voltage of 13 kV, the total x-ray photon energy calculated was about 38 J. The time resolved X-ray signals showed that the pinching of plasma was highly dynamic, that the x-ray signals were extended to about 300 ns with multiple peaks. This explained the higher total yield measured, as opposed to the model calculation of a single peak.

EFFECT OF ARGON PRESSURE ON THE X-RAY YIELD

The effect of filling pressure to the formation of argon plasma was investigated at the charging voltage of 12 kV. The argon pressure was varied from 0.8 mbar to 2.0 mbar. The time resolved x-ray measurements were obtained, and the total x-ray yields were calculated.
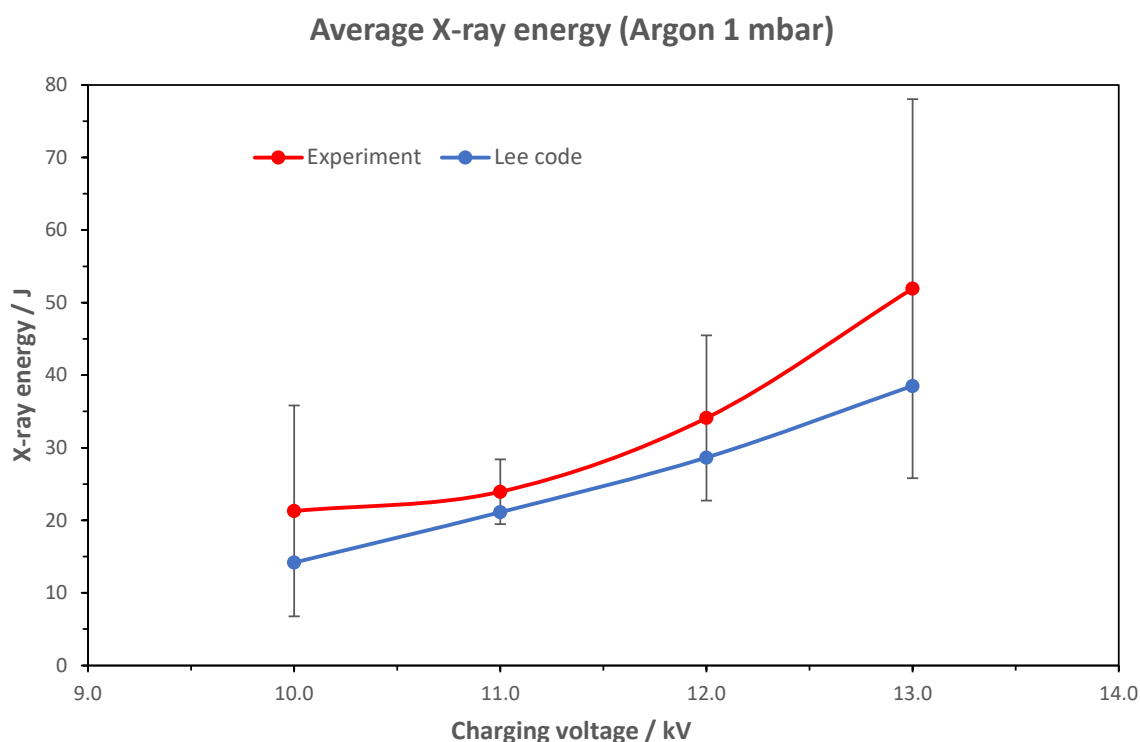

FIGURE 6. Average x-ray energy for the different charging voltage
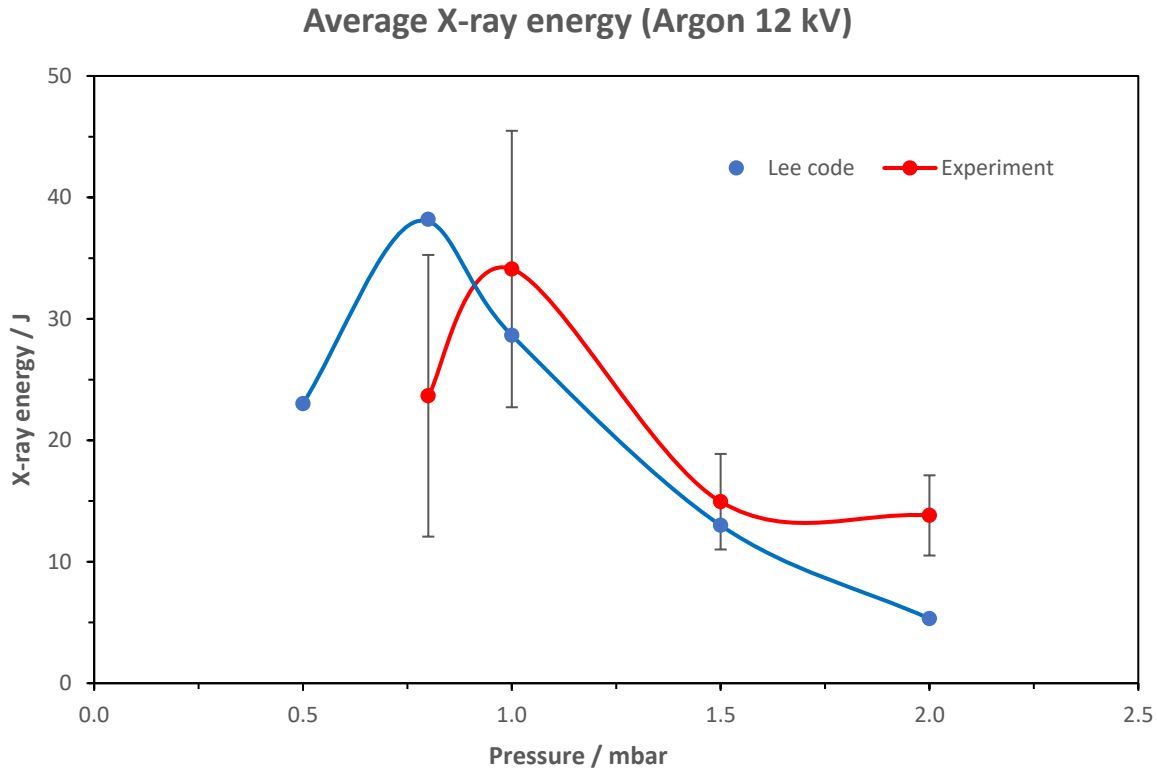
Average X-ray energy (Argon 12 kV)

FIGURE 7. Average x-ray energy obtained from Lee Model for the different operating pressure compared with experiment results

The same experimental conditions were used to obtain the current curve fitting in Lee model, and numerical simulation was carried out. The experimental measured data is plotted in Figure 7. The X-ray emissions increased as pressure increased from 0.8 mbar to 1.0 mbar, beyond which the x-ray yield decreased. The x-ray yields computed by using Lee Model are plotted and compared with the experimental results in Figure 7. Highest x-ray yield was obtained at 1.0 mbar while it was determined at 0.8 mbar according to the numerical calculation. The breakdown and current sheath lift-of phase of the discharge which depend strongly on a minimum required gas density were not considered in the Lee model code, therefore, the 0.8 mbar numerical experiment was calculated with high x-ray yield. In the experimental observation, operation at 0.8 mbar argon was inefficient in the breakdown phase, rendering a poor current sheath formation and leading to a weak plasma pinch formation, thus a low x-ray yield. In practice, the optimum condition for the soft x-ray emission from the argon plasma was determined based on the highest total x-ray photon energy obtained experimentally, it was at

1.0 mbar argon with an average total X-ray photon energy of 34.1±11 J. The result was not significantly different ($p>0.05$) compared to results of other pressures. The standard deviation was calculated from 20 shots.

ELECTRON TEMPERATURE OF THE ARGON PLASMA PINCH

The electron temperature of the argon plasma pinch was obtained from the spectra analysis of the x-ray emission with the filter technique. The calculated curves for electron temperature of 1 keV to 10 keV are plotted in Figure 8. The calculation considered the total x-ray transmission through a set of Ross filters. The same technique was used to obtain the ratio from the measured x-ray signals. At the optimum condition (12 kV, 1 mbar argon) the ratios are plotted and compared to the calculated curves. The time resolved x-ray signals often consist of 4 peaks, correspond to 4 instantaneous pulsed of emissions. The ratios of each peak was calculated. The ratios of the 4 peaks are plotted in Figure 8. The results show that the soft x-rays emission is more than 3 keV. The second peak was higher than 10 keV which may be due to the participation of anode material mixed in the pinching
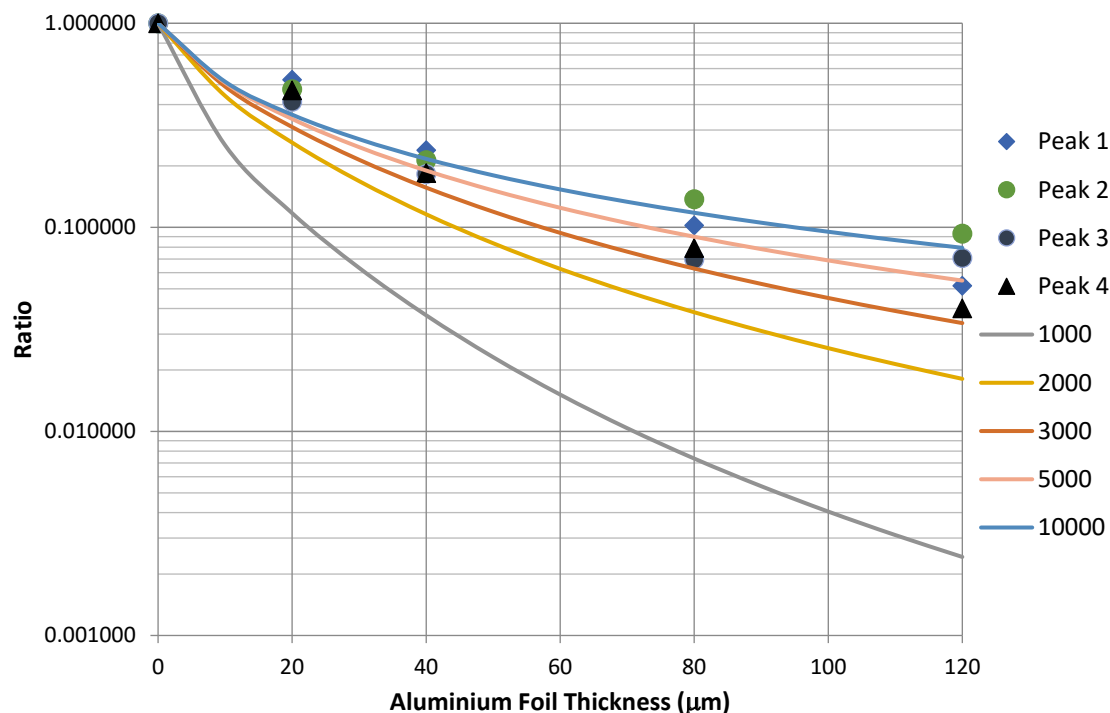
FIGURE 8. Calculated absorption curves of aluminium for X-rays from an argon plasma

plasma. The soft x-ray of 3 keV to 10 keV has a good potential to be considered as soft x-ray radiotherapy.

PLASMA PINCH ENERGY

The discharge voltage and current signals were analysed. The voltage spikes and the current dips which were the signature of the plasma focus pinching were analysed and the dissipated power was obtained. It was observed that the pinch energy increased with the higher charging voltage. The correlation between the pinch energy and charging voltage are shown in Figure 9. About 388 J of pinch energy was recorded at 1 mbar argon discharge at 12 kV, corresponded to 39% of the discharge energy. The obtained x-ray signals shown that there was only about 6.7% passed through the 80 μm aluminium filter with energy above 3 keV, indicated that most of the x-ray emissions produced by PF device at 1 mbar Argon gas with 12 kV of charging voltage were below 3 keV.

RADIATION EFFECT ON NHDF AND MELANOMA B16-F10 CELL

The spectra analysis of the plasma focus emission showed that the soft X-ray was primarily less than 3 keV. The radiation effect of this short pulse of soft x-ray on cells was investigated against the skin melanoma B16-F10 cell and NHDF cell. The cell line samples were irradiated. The plate of the cell line samples were placed at the end-on direction outside the Mylar window as shown in Figure 1. Thin Mylar with thickness of 22.5 micron was used, allowing about 80% transmission of X-ray of above 1 keV. The skin cancer cell and normal cell were irradiated by a single shot of the plasma focus discharge that operated with argon gas at 1 mbar and 12 kV. The maximum x-ray energy received by the cell estimated at 34 J (assuming a point source in $4pr^2$) per shot. The control and irradiated cell samples were incubated up to three days. The cell growths after the soft x-ray irradiation were different in the two types of cells. The reduction in cell growth was more significant to the B16-F10 melanoma cell. The percent cell growth of the control and irradiated cells sample for B16-F10 melanoma cell and NHDF cell are plotted in Figure 10. The obtained results show that the x-ray irradiation inhibited the B16-F10 melanoma cell growth at day 1, statistically significant ($p<0.05$). The results of irradiation on NHDF shown little reduction in the cell growth and statistically insignificant ($p>0.05$), as shown in Table 3.

The results showing a selective effect of the soft x-ray radiation on normal and cancer cells are very interesting, it can be a basis of x-ray radiotherapy. The effect of x-ray radiated on cancer cell is related to the x-ray energy absorption by the cells during the G2/M phase arrest (Liu et al. 2013). It was also reported that a different respond to low dose radiation in the human prostate cells and the prostate cancer cells was believed to be due to some lacking functional and different activating pathway. The effect of a short pulse soft x-ray on cells remain unclear, but it has an inevitably advantage. In the case of skin cancer, a short pulsed soft x-ray can be accurately administrated to the targeted region without stressing the neighbouring cells. Selected x-ray wavelengths or the x-ray spectra for radiotherapy is also an important aspect to be considered, while we have demonstrated the effects of the soft x-ray spectra of a high temperature argon plasma.
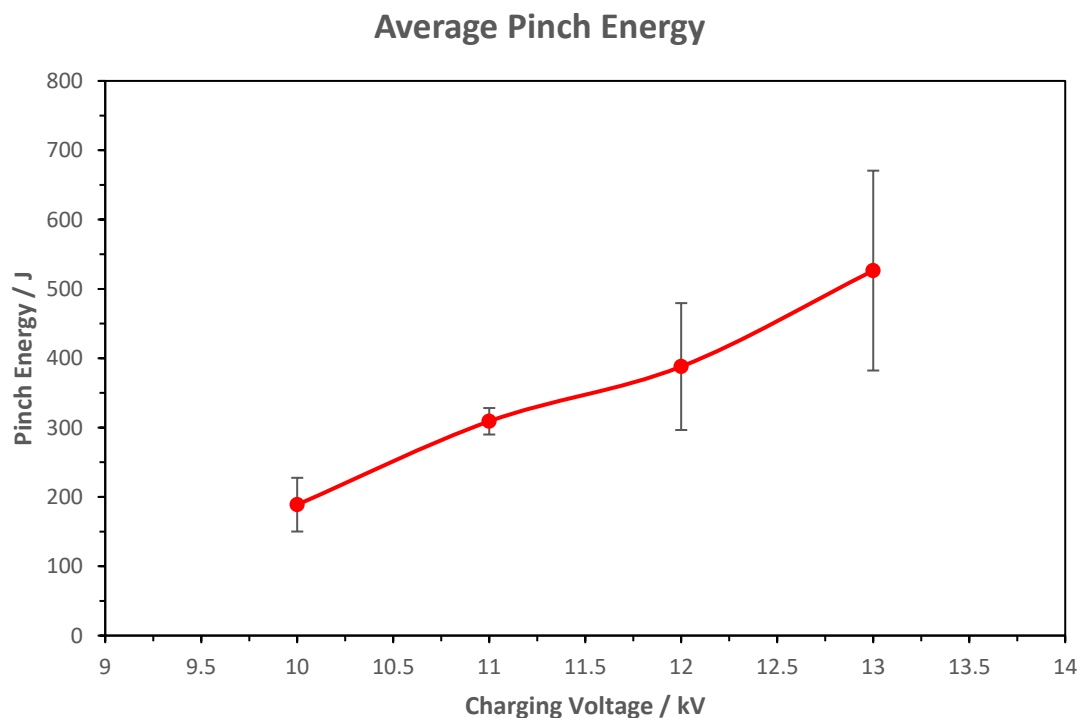

FIGURE 9. Average pinch energy obtained for the different charging voltage

TABLE 3. Percent cell growth of control and treated B16-F10 melanoma cell and NHDF

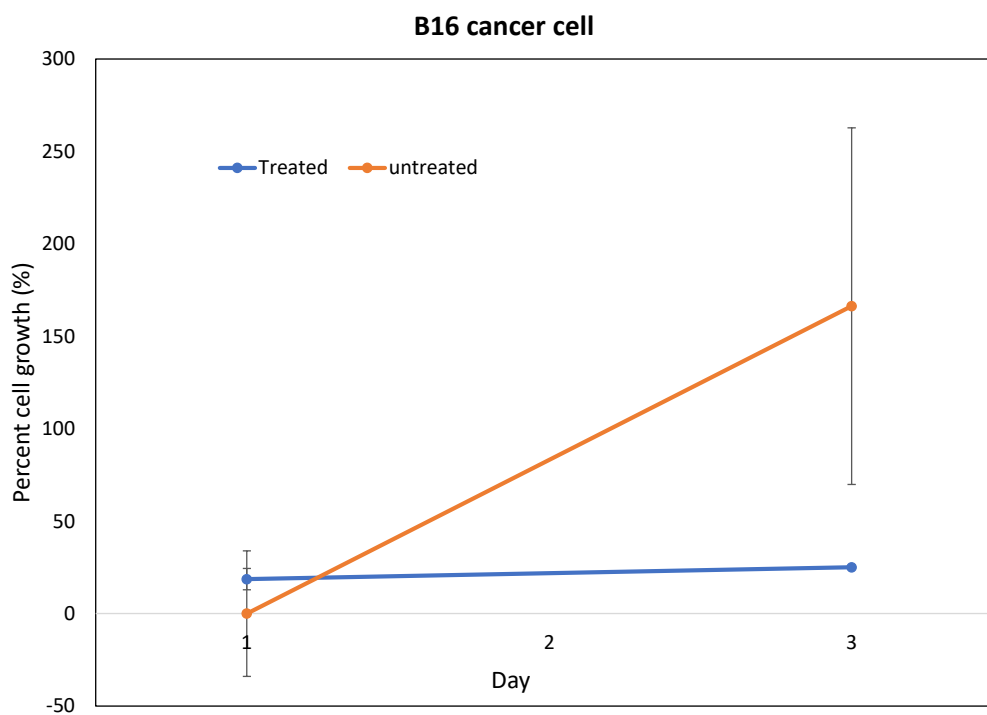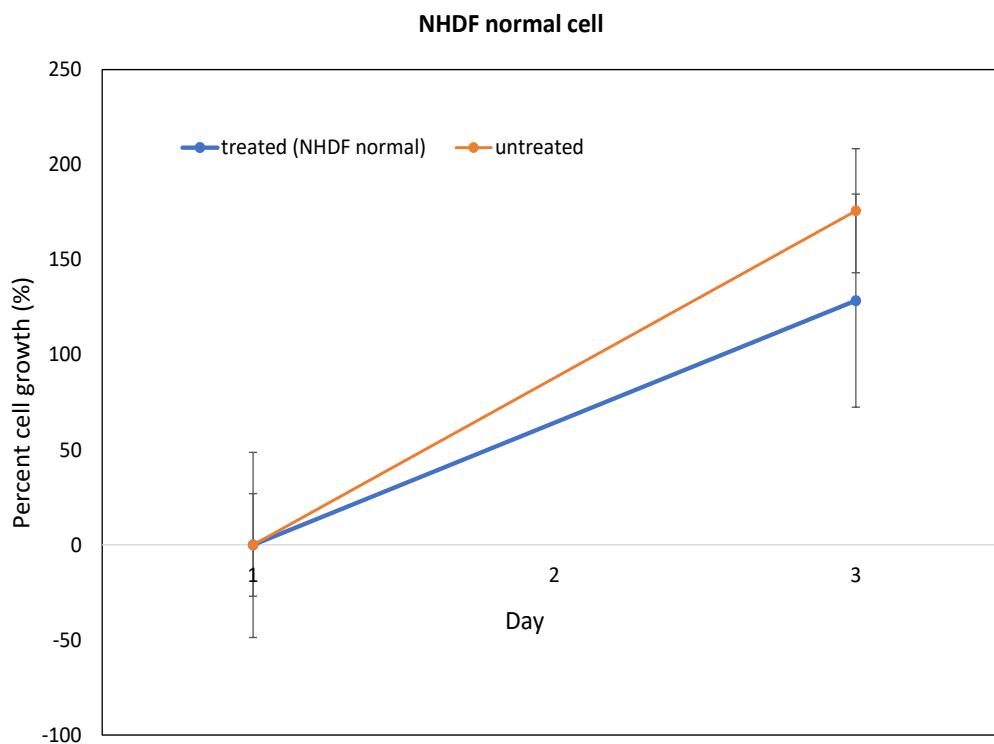|	B16-F10 melanoma cell		NHDF	
	Day 1	Day 3	Day 1	Day 3
Treated	18.65 ± 5.72	25.07 ± 0.94	0.00 ± 26.93	128.51 ± 56.05
Untreated	0.00 ± 33.96	166.32 ± 96.50	0.00 ± 48.66	175.81 ± 32.58
Significance difference	Significant $(p<0.05)$	Not significant $(p>0.05)$	Not significant $(p>0.05)$	Not significant $(p>0.05)$

FIGURE 10. Percent cell growth of control and treated cell samples, (a). the NHDF normal skin cell and (b). B16-F10 melanoma cell, the data on day 1 shown a significant difference (p <0.05)

Conclusion

Argon plasma pinch was produced with the PF discharge operated 1.50 to 2.54 kJ. The x-ray spectra were mainly in the region of 3 keV with some components of higher energy. A single shot of PF discharge produces few tens of joules, measured in the range of 52 J ± 14 J. The plasma pinch characteristic was obtained with reference to the discharge voltage and current signals. A systematic increase in the charging voltage from 10 kV to 13 kV gave the peak current of 95 to 122 kA. The intensity of the x-ray emission also increased with increased charging voltage, with the highest x-ray yield obtained at 13 kV. An optimal condition was searched with the charging voltage of 12 kV, and the argon gas pressure was varied from 0.8 mbar to 2.0 mbar. The x-ray energy measured was maximum at 1 mbar. The x-ray output was compared to a numerical simulated results using the Lee Model code. An average total x-ray photon energy of 28.5 J was obtained at the argon pressure of 1.0 mbar, at 12 kV. The effect of this short pulse soft x-ray on cell lines was evidenced. The skin cancer cell and normal cell NHDF were irradiated and their growths were measured after three days of incubation. The results indicated a different impact of the soft x-ray irradiation on the normal cells and the B16-F10 melanoma cells This could be related to a the different phase arrested induced by the soft x-ray energy as reported by Rainey et al. (2008). Further investigation on the selectivity effect of specific x-ray spectra on cells would be rewarding. The pathways in cell cycle have been intricately connected with the cellular responses to radiation for many years, and lead to the commonly used hard x-ray radiotherapy for cancer treatment. The hard x-ray irradiation also negatively impacts the normal cells, and causes irreparable DNA damage (Jia et al. 2021; Lonati et al. 2021). There are recent study on the application of low dose radiation effects on cell cycle (Khan & Wang 2022), while the roles of the soft x-ray in the cell cycle arrests/enhanced progression remains unclear. Interdisciplinary research on soft x-ray radiotherapy shall be possible making use of the PF generated pulsed x-ray, with the spectra depending on the gas type and temperature in the plasma pinch. The results obtained here with argon plasma at about 3 keV is suitable for superficial irradiation affecting cell growth, with about 50% reduction to the NHDF normal cell and 140% to the B16-F10 melanoma cell.

References

Akel, M., AL-Hawat, S., Ahmad, M., Ballul, Y. & Shaaban, S. 2022. Features of pinch plasma, electron, and ion beams that originated in the AECS PF-1 plasma focus device. *Plasma* 5(2): 184-195.

Ay, Y. 2021. Neon soft x-ray yield optimization in spherical plasma focus device. *Plasma Physics and Controlled Fusion* 63(11): 115009.

Benzi, V., Mezzetti, F., Rocchi, F. & Sumini, M. 2004. Feasibility analysis of a plasma focus neutron source for BNCT treatment of transplanted human liver. *Nuclear Instruments and Methods in Physics Research Section B: Beam Interactions with Materials and Atoms* 213: 611-615.

Bernard, A., Cloth, P., Conrads, H., Coudeville, A., Gourlan, G., Jolas, A., Maisonnier, C. & Rager, J. 1977. The dense plasma focus - A high intensity neutron source. *Nuclear Instruments and Methods* 145(1): 191-218.

Bhuyan, H., Chuaqui, H., Favre, M., Mitchell, I. & Wyndham, E. 2005. Ion beam emission in a low energy plasma focus device operating with methane. *Journal of Physics D: Applied Physics* 38(8): 1164.

Castillo-Mejía, F., Milanese, M.M., Moroso, R.L., Pouzo, J.O. & Santiago, M.A. 2001. Small plasma focus studied as a source of hard X-ray. *IEEE Transactions on Plasma Science* 29(6): 921-926.

Filippov, N., Filippova, T. & Vinogradov, V. 1962. Dense high-temperature plasma in a non-cylindrical Z-pinch compression. *Nucl. Fusion, Suppl.*

Filippov, N.V., Filippova, T.I., Karakin, M.A., Krauz, V.I., Tykshaev, V.P., Vinogradov, V.P., Bakulin, Y.P., Timofeev, V.V., Zinchenko, V.F., Brzosko, J.R. & Brzosko, J.S. 1996. Filippov type plasma focus as intense source of hard X-rays (E/sub x//spl sime/50 keV). *IEEE Transactions on Plasma Science* 24(4): 1215-1223. https://doi.org/10.1109/27.536568

Housley, D., Hahn, E., Narkis, J., Angus, J., Link, A., Conti, F. & Beg, F. 2021. Effect of insulator surface conditioning on the pinch dynamics and x-ray production of a Ne-filled dense plasma focus. *Journal of Applied Physics* 129(22): 223303.

Isolan, L., Sumini, M., Teodori, F., Bradley, D., Jafari, S., Mariotti, F. & Buontempo, F. 2019. Dosimetric analysis and experimental setup design for *in-vivo* irradiation with a Plasma Focus device. *Radiation Physics and Chemistry* 155: 17-21.

Jahoda, F., Little, E., Quinn, W., Sawyer, G. & Stratton, T.F. 1960. Continuum radiation in the x ray and visible regions from a magnetically compressed plasma (Scylla). *Physical Review* 119(3): 843.

Jain, J., Araya, H., Moreno, J., Davis, S., Andaur, R., Bora, B., Pavez, C., Marcelain, K. & Soto, L. 2021. Hyper-radiosensitivity in tumor cells following exposure to low dose pulsed x-rays emitted from a kilojoule plasma focus device. *Journal of Applied Physics* 130(16): 164902.

Jia, C., Wang, Q., Yao, X. & Yang, J. 2021. The role of DNA damage induced by low/high dose ionizing radiation in cell carcinogenesis. *Exploratory Research and Hypothesis in Medicine* 6(4): 177-184.

Kalaiselvi, S.M.P. 2016. Fast miniature plasma focus device: Soft x-rays optimization studies and its application in x-ray lithography. PhD Dissertation (Unpublished).

Khan, M.G.M. & Wang, Y. 2022. Advances in the current understanding of how low-dose radiation affects the cell cycle. *Cells* 11(3): 356.

Knoblauch, P., Raspa, V., Di Lorenzo, F., Clausse, A. & Moreno, C. 2018. Hard X-ray dosimetry of a plasma focus suitable for industrial radiography. *Radiation Physics and Chemistry* 145: 39-42.

Kubes, P., Paduch, M., Auluck, S., Sadowski, M., Cikhardt, J., Klir, D., Kravarik, J., Malir, J., Munzar, V. & Novotný, J. 2023. Observation of filaments in mega-ampere dense plasma focus within pure deuterium by means of simultaneous schlieren and interferometry diagnostics. *Physics of Plasmas* 30(1): 012710.

Lee, S. 2014. Plasma focus radiative model: Review of the Lee model code. *Journal of Fusion Energy* 33: 319-335.

Lim, L-K., Yap, S-L., Nee, C-H. & Yap, S-S. 2021. Dynamics of ion beam emission in a low pressure plasma focus device. *Plasma Physics and Controlled Fusion* 63(3): 035012.

Lim, L., Yap, S., Lim, L., Neoh, Y., Khan, M., Ngoi, S., Yap, S.S. & Lee, S. 2016. Parametric optimisation of plasma focus devices for neutron production. *Journal of Fusion Energy* 35(2): 274-280.

Liu, Q., Schneider, F., Ma, L., Wenz, F. & Herskind, C. 2013. Relative Biologic Effectiveness (RBE) of 50 kV x-rays measured in a phantom for intraoperative tumor-bed irradiation. *International Journal of Radiation Oncology. Biology.Physics* 85(4): 1127-1133. https://doi.org/https://doi.org/10.1016/j.ijrobp.2012.08.005

Lonati, L., Barbieri, S., Guardamagna, I., Ottolenghi, A. & Baiocco, G. 2021. Radiation-induced cell cycle perturbations: A computational tool validated with flow-cytometry data. *Scientific Reports* 11(1): 1-14.

Mather, J.W. 1965. Formation of a high-density deuterium plasma focus. *The Physics of Fluids* 8(2): 366-377.

Miremad, S.M. & Bidabadi, B.S. 2018. Effect of inserted metal at anode tip on formation of pulsed X-ray emitting zone of plasma focus device. *Radiation Physics and Chemistry* 145: 58-63.

Mohammadi, M., Piri, A., Manochehrizadeh, M. & Rawat, R. 2017. Sahand plasma focus emitted more than 35 J in yield neon soft X-ray. *Journal of Fusion Energy* 36(6): 240-245.

Patran, A., Tan, L., Stoenescu, D., Rafique, M., Rawat, R., Springham, S., Tan, T., Lee, P., Zakaullah, M. & Lee, S. 2005. Spectral study of the electron beam emitted from a 3 kJ plasma focus. *Plasma Sources Science and Technology* 14(3): 549.

Poh, H.S., Lee, M.C., Yap, S.S., Teow, S.Y., Bradley, D. & Yap, S.L. 2020. Potential use of plasma focus radiation sources in superficial cancer therapy. *Japanese Journal of Applied Physics* 59(SH): SHHB06.

Rainey, M., Black, E., Zachos, G. & Gillespie, D. 2008. Chk2 is required for optimal mitotic delay in response to irradiation-induced DNA damage incurred in G2 phase. *Oncogene* 27(7): 896-906.

Sumini, M., Isolan, L., Cremonesi, M. & Garibaldi, C. 2019. A Plasma Focus device as ultra-high dose rate pulsed radiation source. Part II: X-ray pulses characterization. *Radiation Physics and Chemistry* 164: 108360.

Tartari, A., Da Re, A., Mezzetti, F., Angeli, E. & De Chiara, P. 2004. Feasibility of X-ray interstitial radiosurgery based on plasma focus device. *Nuclear Instruments and Methods in Physics Research Section B: Beam Interactions with Materials and Atoms* 213: 607-610.

van Paassen, H.L. 1971. A time-resolved ross filter system for measuring x-ray spectra in z-pinch Plasma Focus devices. *Review of Scientific Instruments* 42(12): 1823-1824.

Verma, R., Roshan, M., Malik, F., Lee, P., Lee, S., Springham, S., Tan, T., Krishnan, M. & Rawat, R. 2008. Compact sub-kilojoule range fast miniature plasma focus as portable neutron source. *Plasma Sources Science and Technology* 17(4): 045020.

Yap, S., Wong, C., Choi, P., Dumitrescu, C. & Moo, S. 2005. Observation of two phases of neutron emission in a low energy plasma focus. *Japanese Journal of Applied Physics* 44(11R): 8125.

Zhang, T., Lin, J., Patran, A., Wong, D., Hassan, S., Mahmood, S., White, T., Tan, T., Springham, S. & Lee, S. 2007. Optimization of a plasma focus device as an electron beam source for thin film deposition. *Plasma Sources Science and Technology* 16(2): 250.

*Corresponding author; email: yapsl@um.edu.my